

Reconciling the HESS J1731-347 constraints with Parity doublet model

Bikai Gao,^{1,*} Yan Yan,^{2,†} and Masayasu Harada^{3,1,4,‡}

¹*Department of Physics, Nagoya University, Nagoya 464-8602, Japan*

²*School of Microelectronics and Control Engineering, Changzhou University, Jiangsu 213164, China*

³*Kobayashi-Maskawa Institute for the Origin of Particles and the Universe, Nagoya University, Nagoya, 464-8602, Japan*

⁴*Advanced Science Research Center, Japan Atomic Energy Agency, Tokai 319-1195, Japan*

(Dated: April 9, 2024)

The recent discovery of a central compact object (CCO) within the supernova remnant HESS J1731-347, characterized by a mass of approximately $0.77_{-0.17}^{+0.20} M_{\odot}$ and a radius of about $10.4_{-0.78}^{+0.86}$ km, has opened up a new window for the study of compact objects. This CCO is particularly intriguing because it is the lightest and smallest compact object ever observed, raising questions and challenging the existing theories. To account for this light compact star, a mean-field model within the framework of parity doublet structure is applied to describe the hadron matter. Inside the model, part of the nucleon mass is associated with the chiral symmetry breaking while the other part is from the chiral invariant mass m_0 which is insensitive to the temperature/density. The value of m_0 affects the nuclear equation of state for uniform nuclear matter at low density and exhibits strong correlations with the radii of neutron stars. We point out that HESS J1731-347 can be explained as the lightest neutron star for $m_0 \simeq 850$ MeV.

I. INTRODUCTION

Neutron star (NS) is one of the most compact objects in the universe with a mass of $1-2M_{\odot}$ and a radius of ~ 10 km. The NSs with extreme conditions provide us unique natural laboratory for investigating the phases of cold, dense matter, including the possibility of exotic states such as hyperons and even quarks appearing within these astrophysical objects. Understanding the properties of NSs requires the information about its equation of state (EOS) which characterizes how pressure P varies as a function of energy density ϵ . This EOS cannot be directly predicted by the quantum chromodynamics (QCD) and also the lattice QCD simulations due to the sign problem. Thanks to the advancements of recent multi-messenger astronomy on different sources, especially those made by gravitational wave laser interferometers from the LIGO-VIRGO[1-3] and X-ray emissions observations conducted by the Neutron Star Interior Composition Explorer (NICER), we made remarkable improvements to constrain the EOS of cold, dense and strongly interacting nuclear matter. For instance, the NS merger event GW170817 provided insights into the mass and radius of NSs, with an estimation of approximately $1.4M_{\odot}$ and a radius of $R = 11.9_{-1.4}^{+1.4}$ km. This observation suggested that the EOS should be relatively soft for uniform nuclear matter existing in the low-density region. Additionally, NICER has played a crucial role in advancing our understandings of NSs. The analyses[4, 5] have focused on NSs with masses around $1.4M_{\odot}$ and $\sim 2.1M_{\odot}$. Interestingly, the results indicated

that the radii of these NSs are rather similar for different masses, with a radius of approximately 12.45 ± 0.65 kilometers for a $1.4 M_{\odot}$ NS and 12.35 ± 0.75 kilometers for a $2.08 M_{\odot}$ NS. These findings suggest that the EOS stiffens rapidly, meaning that the pressure increases quickly as a function of energy density, as one moves from low baryon density ($\lesssim 2n_0$; n_0 : nuclear saturation density) to high density ($4-7n_0$). This stiffening of the EOS is necessary to support the existence of massive NSs, such as those with masses around $2M_{\odot}$.

The recent report on the central compact object (CCO) HESS J1731-347[6] with an estimated mass and radius of the object are $M = 0.77_{-0.17}^{+0.20} M_{\odot}$ and $R = 10.4_{-0.78}^{+0.86}$ km, have raised many questions and put more constraints into the EOS. This measurements suggest that this CCO may correspond to a neutron star with an even softer equation of state in the low-density region than previously observed. Some studies considered the possibility that HESS J1731-347 may be a quark star[7-10], an exotic theoretical object composed of deconfined quarks rather than the usual hadronic matter suggested in neutron stars.

In this research, we will explore the possibility that HESS J1731-347 may be the neutron star within the framework of a quark-hadron crossover model constructed in [11-14], in which a unified EOS is constructed by interpolating the hadronic EOS from a hadronic model based on the parity doublet structure[15, 16]. and the quark EOS from an NJL-type quark model.

Hadronic models based on the parity doublet structure, which we call parity doublet models(PDMs), offer a unique perspective on the structure of hadrons by considering the existence of chiral invariant mass, denoted by m_0 , in addition to the conventional chiral variant mass generated by the spontaneous chiral symmetry breaking. The existence of the chiral invariant mass is consistent with the lattice QCD simulation done at

* gaobikai@hken.phys.nagoya-u.ac.jp

† 2919ywhhxh@163.com

‡ harada@hken.phys.nagoya-u.ac.jp

non-zero temperature [17]. The framework of PDMs has been widely used to study the hadron structure[18–22] and construct the EOS for nuclear /NS matter[11–14, 23–46]. We note that the constructed EOS is softer for larger chiral invariant mass, and the resultant EOSs are combined with the EOS constructed from an NJL-type quark model by assuming quark-hadron crossover, which allows for a smooth transition from hadronic matter to quark matter[11–14, 44, 45]. This hybrid approach, where the PDM EOS is employed up to densities around $2\text{--}3n_0$ and interpolate with the quark EOS at $\geq 5n_0$ via polynomial interpolation to obtain the unified EOS. In this case, the unified EOS can be constructed with soft EOS in the low density part and sufficiently stiff EOS in the high density part to support the $2M_\odot$ constraint.

In this work, we consider a hadronic EOS constructed from a PDM in the low density region and interpolate with quark EOS using an NJL-type quark model in the high density region. Inside the PDM, we included the $\rho^2\omega^2$ interaction term with $\lambda_{\omega\rho}$ to be its coupling constant, which is assumed to make the EOS softer. By adjusting the two parameters $\lambda_{\omega\rho}$ and m_0 , we can adjust the stiffness of EOS in the hadronic model. The constructed unified EOS is shown to satisfy the constraints from HESS J1731-347, makes it possible to be the lightest neutron star ever observed.

This paper is organized as follows. In Sec. II, we explain the formulation of present model. The main results of the analysis of properties of NS are shown in Sec. III. Finally, we show the summary and discussions in Sec. IV.

II. EQUATION OF STATE

In this section, we briefly review how to construct neutron star matter EOS from a PDM in the low-density region, and from a NJL-type quark model in the high-density region.

A. NUCLEAR MATTER EOS

In Ref. [14], a hadronic parity doublet model (PDM) is constructed to describe the NS properties in the low density region ($\leq 2n_0$). The model includes the effects of strange quark chiral condensate through the KMT-type interaction in the mesonic sector. The density dependence of the strange quark chiral condensate $\langle\bar{s}s\rangle$ is calculated and the results show the impacts of strange quark chiral condensate is very limited in the low density region. Then, in the current study, we neglect the effect of strange quark in the low density domain. In addition, we ignore the influence of the isovector scalar meson $a_0(980)$ in the current model, which believed to appear in asymmetric matter like neutron stars. As investigated in Ref. [46], the effect of the $a_0(980)$ has a negligible impact on the properties of neutron stars. Specifically, the inclusion of the $a_0(980)$ only results in a slight

increase in the radius by less than a kilometer. We would like also to note that, in these analyses, a term of vector meson mixing, i.e. $\omega^2\rho^2$ term, is introduced to make the slope parameter to be consistent with the recent constraint shown in Ref. [47]. In the present analysis, we also include the mixing contribution.

The thermodynamic potential is obtained as [38, 40]

$$\begin{aligned} \Omega_{\text{PDM}} = & V(\sigma) - V(\sigma_0) - \frac{1}{2}m_\omega^2\omega^2 - \frac{1}{2}m_\rho^2\rho^2 \\ & - \lambda_{\omega\rho}(g_\omega\omega)^2(g_\rho\rho)^2 \\ & - 2 \sum_{i=+,-} \sum_{\alpha=p,n} \int^{k_f} \frac{d^3\mathbf{p}}{(2\pi)^3} (\mu_\alpha^* - E_{\mathbf{p}}^i), \end{aligned} \quad (1)$$

where $i = +, -$ denote the parity of nucleons and $E_{\mathbf{p}}^i = \sqrt{\mathbf{p}^2 + m_i^2}$ is the energy of nucleons with mass m_i and momentum \mathbf{p} . In Eq (1), the potential $V(\sigma)$ is given by

$$V(\sigma) = -\frac{1}{2}\bar{\mu}^2\sigma^2 + \frac{1}{4}\lambda_4\sigma^4 - \frac{1}{6}\lambda_6\sigma^6 - m_\pi^2 f_\pi \sigma, \quad (2)$$

and σ_0 is the mean field at vacuum.

We note that the sign of λ is restricted to be positive due to the stability of the vacuum at zero density[46]. The total thermodynamic potential for the NS is obtained by including the effects of leptons as

$$\Omega_{\text{H}} = \Omega_{\text{PDM}} + \sum_{l=e,\mu} \Omega_l, \quad (3)$$

where $\Omega_l(l = e, \mu)$ are the thermodynamic potentials for leptons given by

$$\Omega_l = -2 \int^{k_f} \frac{d^3\mathbf{p}}{(2\pi)^3} (\mu_l - E_{\mathbf{p}}^l). \quad (4)$$

The mean fields here are determined by following stationary conditions:

$$0 = \frac{\partial\Omega_{\text{H}}}{\partial\sigma}, \quad 0 = \frac{\partial\Omega_{\text{H}}}{\partial\omega}, \quad 0 = \frac{\partial\Omega_{\text{H}}}{\partial\rho}. \quad (5)$$

We also need to consider the β equilibrium and the charge neutrality conditions,

$$\mu_e = \mu_\mu = -\mu_Q, \quad (6)$$

$$\frac{\partial\Omega_{\text{H}}}{\partial\mu_Q} = n_p - n_l = 0, \quad (7)$$

where μ_Q is the charge chemical potential. We then have the pressure in hadronic matter as

$$P_{\text{H}} = -\Omega_{\text{H}}. \quad (8)$$

We then determine the parameters in the PDM by fitting them to the pion decay constant and hadron masses given in Table. I and the normal nuclear matter properties summarized in Table. II for fixed value of m_0 . In addition, we use the slope parameter as an input to

TABLE I: Physical inputs in vacuum in unit of MeV.

m_π	f_π	m_ω	m_ρ	m_+	m_-
140	92.4	783	776	939	1535

TABLE II: Saturation properties used to determine the model parameters: the saturation density n_0 , the binding energy B_0 , the incompressibility K_0 , symmetry energy S_0 .

n_0 [fm^{-3}]	E_{Bind} [MeV]	K_0 [MeV]	S_0 [MeV]
0.16	16	240	31

determine the coefficient $\lambda_{\omega\rho}$ of the ω - ρ mixing term. In the present analysis, we need to use the slope parameter as an input to determine the strength of the vector meson mixing (namely the parameter $\lambda_{\rho\omega}$). The estimation in Ref. [47] provide the best value is $L = 57.7 \pm 19$ MeV.

For studying this sensitivity, we first study the EOSs for $L = 40, 57.7, 70, 80$ MeV with $m_0 = 800$ MeV fixed.

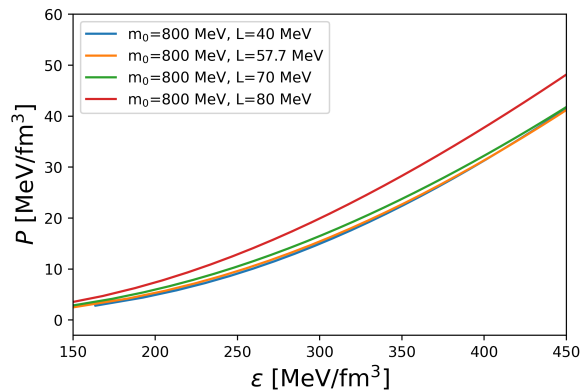
In Table. III, we summarize the values of the parameters $g_{\rho NN}$ and $\lambda_{\omega\rho}$ for several choices of the chiral invariant mass and the slope parameter. Since the introduc-

TABLE III: Determined values of $\lambda_{\omega\rho}$ and $g_{\rho NN}$ with different choices of the chiral invariant mass m_0 and the slope parameter L .

$L = 40$ MeV					
m_0 [MeV]	500	600	700	800	900
$\lambda_{\omega\rho}$	0.045	0.087	0.192	0.504	3.243
$g_{\rho NN}$	7.31	7.85	8.13	8.30	8.43
$L = 57.7$ MeV					
m_0 [MeV]	500	600	700	800	900
$\lambda_{\omega\rho}$	0.037	0.066	0.141	0.362	2.28
$g_{\rho NN}$	7.31	7.85	8.13	8.30	8.43
$L = 70$ MeV					
m_0 [MeV]	500	600	700	800	900
$\lambda_{\omega\rho}$	0.028	0.045	0.088	0.211	1.252
$g_{\rho NN}$	7.31	7.85	8.13	8.30	8.43
$L = 80$ MeV					
m_0 [MeV]	500	600	700	800	900
$\lambda_{\omega\rho}$	0.020	0.021	0.025	0.030	0.013
$g_{\rho NN}$	7.31	7.85	8.13	8.30	8.43

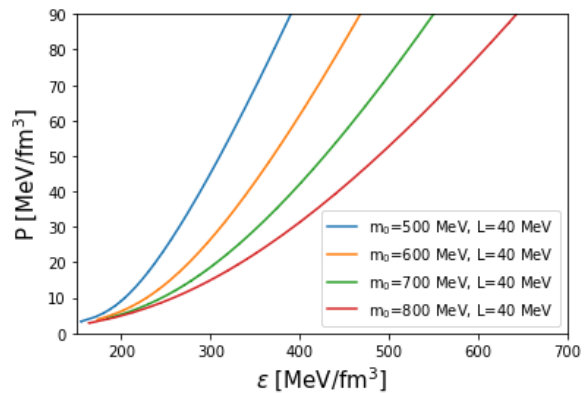
tion of ω - ρ mixing does not have impacts on the normal nuclear matter construction, the coupling constants of scalar mesons, $\bar{\mu}^2$, λ_4 and λ_6 are exactly same as those determined in Ref. [40], we only list the values for the $\lambda_{\omega\rho}, g_{\rho NN}$.

The dependence on the slope parameter L for $m_0 = 800$ MeV is plotted in Fig. 1. This shows that the smaller L leads to softer EOS as expected. As we will show later, we need very soft EOS in the low density region to

FIG. 1: EOS for different values of the slope parameter L for $m_0 = 800$ MeV.

reproduce the HESS data. Then, we will take $L = 40$ MeV as a typical choice in the preceding analysis.

We can then calculate the EOS in the hadronic model and the corresponding EOS for PDM with fixing slope parameter $L = 40$ MeV is shown in Fig. 2. From this

FIG. 2: EOS for different values of m_0 for $L = 40$ MeV.

figure, we easily find that larger values of m_0 lead to softer EOSs. This is understood as follows: a greater m_0 leads to a weaker σ coupling to nucleons, because a nucleon does not have to acquire its mass entirely from the σ fields. The couplings to ω fields are also smaller because the repulsive contributions from ω fields must be balanced with attractive σ contributions at the saturation density n_0 . At densities larger than n_0 , however, the σ field reduces but the ω field increases, and these contributions are no longer balanced, affecting the stiffness of the EOS.

B. QUARK MATTER EOS

Following Refs.[11, 48], we use an NJL-type quark model to describe the quark matter. The model includes three-flavors and $U(1)_A$ anomaly effects through the

quark version of the KMT interaction. The coupling constants are chosen to be the Hatsuda-Kunihiro parameters which successfully reproduce the hadron phenomenology at low energy [11, 49]: $G\Lambda^2 = 1.835$, $K\Lambda^5 = 9.29$ with $\Lambda = 631.4$ MeV, see the definition below. The couplings g_V and H characterize the strength of the vector repulsion and attractive diquark correlations whose range will be examined later when we discuss the NS constraints.

We can then write down the thermodynamic potential as

$$\Omega_{\text{CSC}} = \Omega_s - \Omega_s [\sigma_f = \sigma_f^0, d_j = 0, \mu_q = 0] + \Omega_c - \Omega_c [\sigma_f = \sigma_f^0, d_j = 0], \quad (9)$$

where the subscript 0 is attached for the vacuum values, and

$$\Omega_s = -2 \sum_{i=1}^{18} \int^{\Lambda} \frac{d^3\mathbf{p}}{(2\pi)^3} \frac{\epsilon_i}{2}, \quad (10)$$

$$\Omega_c = \sum_i (2G\sigma_i^2 + Hd_i^2) - 4K\sigma_u\sigma_d\sigma_s - g_V n_q^2, \quad (11)$$

with σ_f being the chiral condensates, d_j denotes for diquark condensates, and n_q denotes for the quark density. In Eq.(10), ϵ_i are energy eigenvalues obtained from inverse propagator in Nambu-Gorkov bases

$$S^{-1}(k) = \begin{pmatrix} \gamma_\mu k^\mu - \hat{M} + \gamma^0 \hat{\mu} & \gamma_5 \sum_i \Delta_i R_i \\ -\gamma_5 \sum_i \Delta_i^* R_i & \gamma_\mu k^\mu - \hat{M} - \gamma^0 \hat{\mu} \end{pmatrix}, \quad (12)$$

where

$$\begin{aligned} M_i &= m_i - 4G\sigma_i + K |\epsilon_{ijk}| \sigma_j \sigma_k, \\ \Delta_i &= -2Hd_i, \\ \hat{\mu} &= \mu_q - 2g_V n_q + \mu_3 \lambda_3 + \mu_8 \lambda_8 + \mu_Q Q, \\ (R_1, R_2, R_3) &= (\tau_7 \lambda_7, \tau_5 \lambda_5, \tau_2 \lambda_2). \end{aligned} \quad (13)$$

$S^{-1}(k)$ is 72×72 matrix in terms of the color, flavor, spin, and Nambu-Gorkov basis, which has 72 eigenvalues. $M_{u,d,s}$ are the constituent masses of u, d, s quarks and $\Delta_{1,2,3}$ are the gap energies. The $\mu_{3,8}$ are the color chemical potentials which will be tuned to achieve the color neutrality. The total thermodynamic potential including the effect of leptons is

$$\Omega_Q = \Omega_{\text{CSC}} + \sum_{l=e,\mu} \Omega_l. \quad (14)$$

The mean fields are determined from the gap equations,

$$0 = \frac{\partial \Omega_Q}{\partial \sigma_i} = \frac{\partial \Omega_Q}{\partial d_i}, \quad (15)$$

From the conditions for electromagnetic charge neutrality and color charge neutrality, we have

$$n_j = -\frac{\partial \Omega_Q}{\partial \mu_j} = 0, \quad (16)$$

where $j = 3, 8, Q$. The baryon number density n_B is determined as

$$n_q = -\frac{\partial \Omega_Q}{\partial \mu_q}, \quad (17)$$

where μ_q is 1/3 of the baryon number chemical potential. After determined all the values, we obtain the pressure as

$$P_Q = -\Omega_Q. \quad (18)$$

III. STUDY OF PROPERTIES OF NS

In this section, following Ref. [40] we construct a unified EOS by connecting the EOS obtained in the PDM introduced in Sec. II A and the EOS of NJL-type quark model given in Sec. II B, and solve the TOV equation [50, 51] to obtain the NS mass-radius (M - R) relation. As for the interplay between nuclear and quark matter EOS, see, e.g., Ref. [52] for a quick review that classifies types of the interplay.

A. Construction of unified EOS

$0 \leq n_B < 0.5n_0$	$0.5n_0 \leq n_B \leq 2n_0$	$2n_0 < n_B < 5n_0$	$n_B \geq 5n_0$
Crust	PDM	Interpolation	NJL

TABLE IV: Unified EOS composed of four part.

In our unified equations of state as in Table.IV, we use the BPS (Baym-Pethick-Sutherland) EOS [53] as a crust EOS for $n_B \lesssim 0.5n_0$. From $n_B \simeq 0.5n_0$ to $2n_0$ we use our PDM model to describe a nuclear matter. We limit the use of our PDM up to $2n_0$ so that baryons other than ground state nucleons, such as the negative parity nucleons or hyperons, do not show up in matter. Beyond $2n_0$ nuclear regime, we assume a crossover from the nuclear matter to quark matter, and use a smooth interpolation to construct the unified EOS. We expand the pressure as a fifth order polynomial of μ_B as

$$P_I(\mu_B) = \sum_{i=0}^5 C_i \mu_B^i, \quad (19)$$

where C_i ($i = 0, \dots, 5$) are parameters to be determined from boundary conditions given by

$$\begin{aligned} \left. \frac{d^n P_I}{(d\mu_B)^n} \right|_{\mu_{BL}} &= \left. \frac{d^n P_H}{(d\mu_B)^n} \right|_{\mu_{BL}}, \\ \left. \frac{d^n P_I}{(d\mu_B)^n} \right|_{\mu_{BU}} &= \left. \frac{d^n P_Q}{(d\mu_B)^n} \right|_{\mu_{BU}}, \quad (n = 0, 1, 2), \end{aligned} \quad (20)$$

with μ_{BL} being the chemical potential corresponding to $n_B = 2n_0$ and μ_{BU} to $n_B = 5n_0$. We demand the matching up to the second order derivatives of pressure at each boundary. The resultant interpolated EOS must satisfy the thermodynamic stability condition,

$$\chi_B = \frac{\partial^2 P}{(\partial \mu_B)^2} \geq 0, \quad (21)$$

and the causality condition,

$$c_s^2 = \frac{dP}{d\varepsilon} = \frac{n_B}{\mu_B \chi_B} \leq 1, \quad (22)$$

which means that the sound velocity is smaller than the light velocity. These conditions restrict the range of quark model parameters (g_V, H) for a given nuclear EOS and a choice of (n_L, n_U) . We exclude interpolated EOSs which do not satisfy the above-mentioned constraints.

B. Mass-Radius relation

In this section, we calculate mass-radius relation of NSs by using the unified EOS constructed in the previous section for the PDM with different parameter choices of chiral invariant mass m_0 and slope parameter L .

First, we study whether the smooth connection is realized depending on the parameters H and g_V in the NJL-type quark model as shown in Fig. 3 for PDM with $L = 40$ MeV. For each combination of (H, g_V) , the cross mark are the parameter choices forbidden by the causality and thermodynamic stability conditions. For possible choices of (H, g_V) , we determine the maximum mass of a NS, which is indicated by the color in Fig. 3. This shows that a larger g_V or/and a smaller H leads to a larger maximum mass. For $m_0 = 900$ MeV, the maximum mass for all the choices of (H, g_V) are below $2M_\odot$, leading to the conclusion that $m_0 = 900$ should be excluded when slope parameter is chosen to be $L = 40$ MeV.

In Fig. 4, we fix the value of m_0 with different choice of L and calculate the corresponding mass-radius curves, where the values of (H, g_V) are chosen to have the stiffest EOS. In this figure, the thick part indicates that the density region is smaller than $2n_0$ or larger than $5n_0$ and the thin line indicates the interpolated region. From the figure, for $m_0 = 800$ MeV, the radius for $L = 40$ MeV, $M \simeq 1.4M_\odot$ is about 11.5 km while the result of $L = 80$ MeV about 12.6 km. This result indicates that EOSs are softened by the effect of the $\omega\rho$ interaction. One can see that the M - R curve for $L = 40$ MeV satisfies the constraint from the HESS J1731-347 observation. We note that $L = 40$ MeV is consistent with the one obtained in Ref. [47], due to a large ambiguity. Precise determination of slope parameter in future will help us to further constrain the NS properties.

To achieve a NS with small radius, the outer core EOS (Density around $1n_0$ - $2n_0$) is extremely important, since it directly connects to the radius of a neutron star. In

our model, the chiral invariant mass m_0 and the slope parameter L are two factors which have impacts on the outer core EOS. We then treat them as free parameters and compare the corresponding M - R curves with NS constraints from NICER, gravitational wave detection and HESS. We show the allowed region of m_0 and L satisfying all the observational constraints in 1σ and 2σ range as in Fig. 5. Under this parameter space favoring large m_0 and small L , HESS J1731-347 can be considered as the lightest NS.

IV. SUMMARY AND DISCUSSIONS

In this study, we use parity doublet model together with NJL-type model within the framework of relativistic mean-field model to describe low-mass neutron stars. We construct EOS for NS matter by interpolating the EOS obtained in the PDM and the one in the NJL-type model with assuming the crossover from hadronic matter to quark matter. In the calculation of the NS mass-radius relation, we find outer core EOS is crucial to determine the radius of a NS. Consequently, the choices of chiral invariant mass m_0 and slope parameter L which describe the properties of the uniform nuclear matter are essential. We treat m_0 and L as two free parameters and find the parameter space enable us to explain the HESS J1731-347 as a neutron star as in Fig. 5.

We note here that the typical estimate of L falls within the range of 40-80 MeV, as indicated by various studies[47, 54, 55]. However, there are also other estimates such as $L = (109 \pm 36.41)$ MeV derived from the analyses of neutron skin thickness from PREX-2 experiment. There is still large ambiguities about the value of slope parameter. In the present research, we follow Ref. [47] as the baseline to set $L = 57.7 \pm 19$ MeV and study the corresponding mass-radius relation. If future experiment show the value of slope parameter is large, we can come to the conclusion that HESS J1731-347 cannot be explained as a NS within the present model.

As studied in Refs.[56–58], the validity of pure hadronic descriptions at $n_B \geq 2n_0$ are questionable as nuclear many-body forces are very important, implying that quark descriptions are required even before the quark matter formation. In this study, we choose the interpolation point to be $2n_0$ and the ambiguity from the interpolation point is discussed in Fig. 6. In this figure, we show the M - R curves for $m_0 = 850$ MeV and $L = 40$ MeV with changing the interpolation range from $2n_0$ - $5n_0$ to $1.5n_0$ - $5n_0$ and $2.5n_0$ - $5n_0$. We can easily see that the ambiguity from the interpolation point is very limited: at the mass about $1M_\odot$, the radius shifts are only about 0.1 km.

In Fig. 7, we fix the value of slope parameter as $L = 40$ MeV and vary the value of m_0 as $m_0 = 600, 700, 800$ MeV. We choose the values of (H, g_V) parameters to produce the most stiff and the most soft EOSs satisfying $2M_\odot$ constraint. For $m_0 = 700, 800$ MeV, the rather

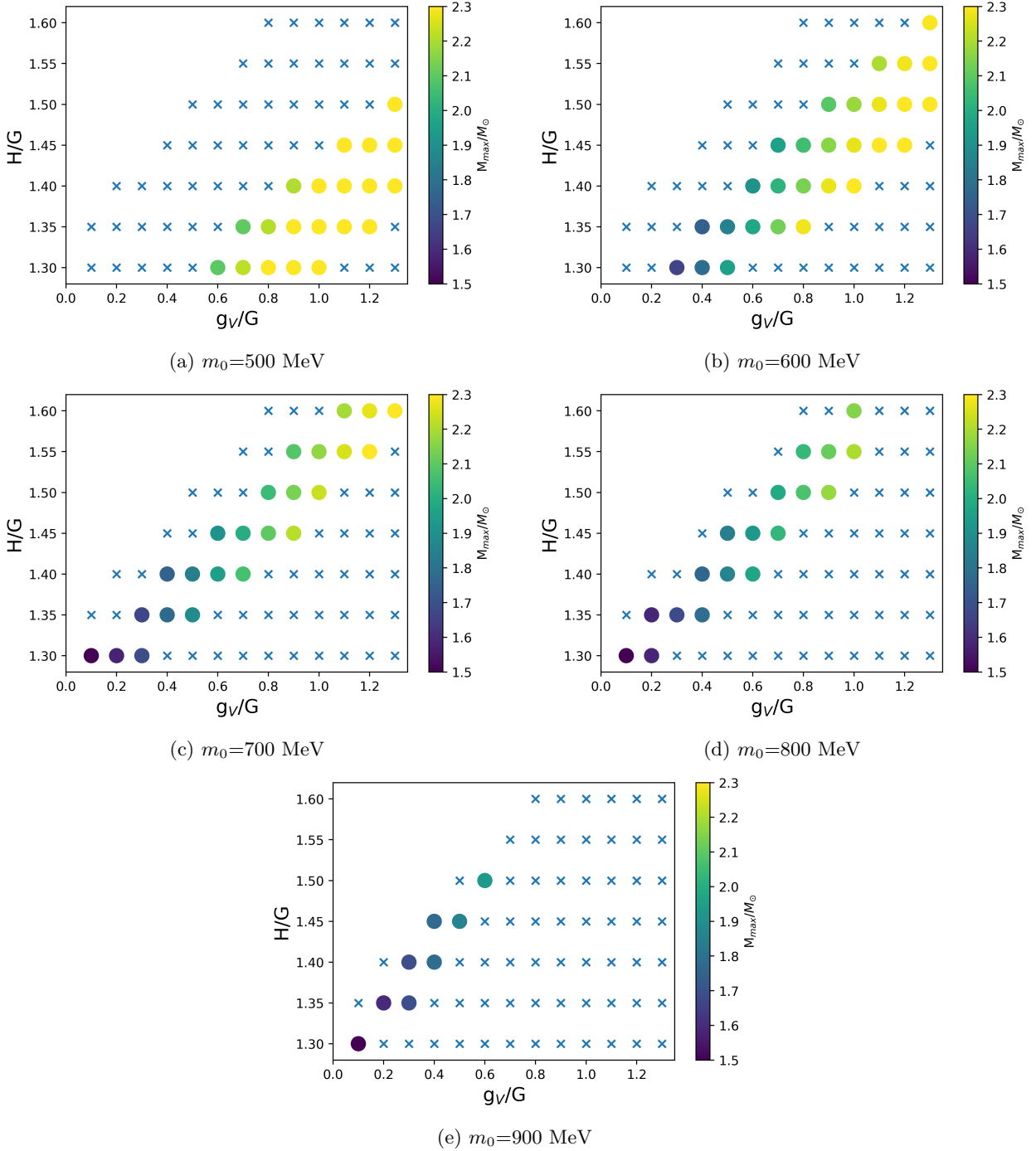


FIG. 3: Allowed combination of (H, g_V) values for $m_0 = 500, 600, 700, 800, 900$ MeV when $L = 40$ MeV. Cross mark indicates that the combination of (H, g_V) is excluded by the causality constraints. Circle indicates that the combination is allowed. The color shows the maximum mass of NS obtained from the corresponding parameters, as indicated by a vertical bar at the right side of each figure.

soft hadronic EOSs are connected with rather stiff quark EOSs satisfying $2M_\odot$ constraint, resulting a peak of the density dependence of sound velocity, as shown in Fig. 8. However, for $m_0 = 600$ MeV, the rather stiff hadronic EOS is used to connect with stiff quark EOSs, resulting

just a bump-like structure. Besides, we find that the onset density of the sound velocity peak is larger for larger m_0 . Reference [59] pointed out that the appearance of the maximum in the speed of sound in the interior of NSs might indicate the change of medium composition,

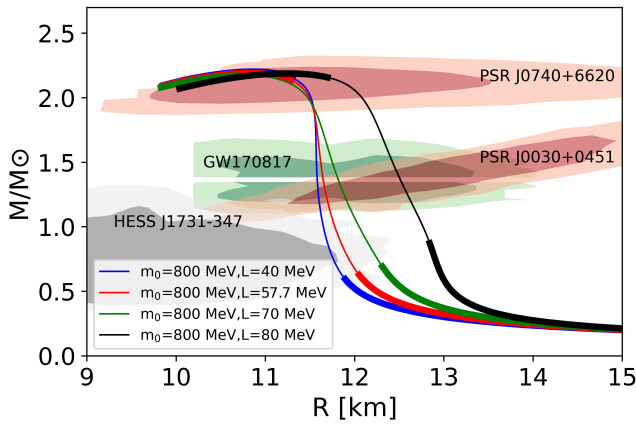


FIG. 4: Mass-radius relations for same $m_0 = 800$ MeV in different PDM sets. Black curve is connected to the NJL parameters $(H, g_V)/G = (1.5, 1)$; green curve to $(H, g_V)/G = (1.55, 1)$; red curve to $(H, g_V)/G = (1.55, 1)$; blue curve to $(H, g_V)/G = (1.55, 1)$.

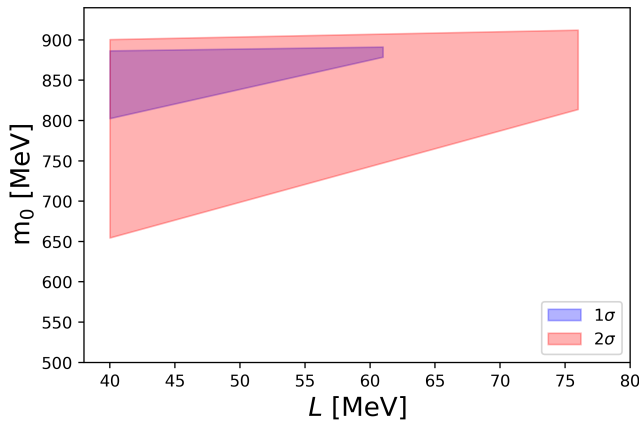


FIG. 5: Allowed region for m_0 and L . Within the shadowed region, the M-R curve satisfy all the constraint from the NS observation within the error of 1σ or 2σ .

from hadronic to quark or quarkyonic matter. They estimate the critical density where baryons begin to overlap as $n_c^{per} = 1.22/V_0$, $V_0 = (4/3)\pi R_0^3$ [60]. After using experimental value of the proton radius $R_0 = 0.9 \pm 0.05$ fm[61, 62], the critical density is calculated as $n_c^{per} = 0.57^{+0.12}_{-0.09}$ fm $^{-3}$. When we require that the peak density of the sound velocity in the present analysis should satisfy $0.48 \leq n_B^{\text{peak}} \leq 0.69$, i.e. $3 \leq n_B^{\text{peak}}/n_0 \leq 4.3$, we obtain the constraint to the chiral invariant mass as

$600 \lesssim m_0 \lesssim 800$ MeV for $L = 40$ MeV.

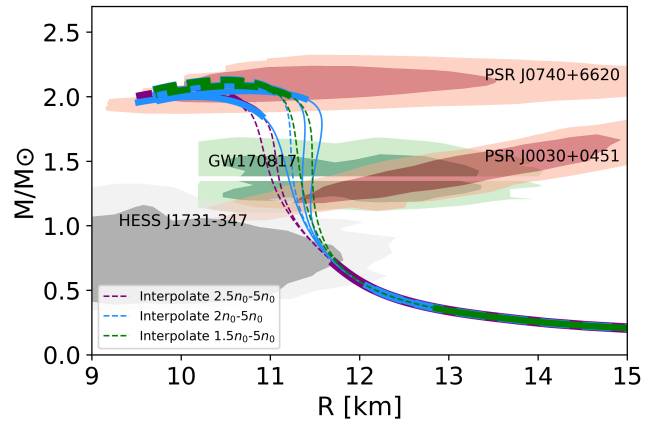


FIG. 6: Mass-radius relations for $m_0 = 850$ MeV, $L = 40$ MeV and corresponding curves for central density. Different colors indicate different interpolation range.

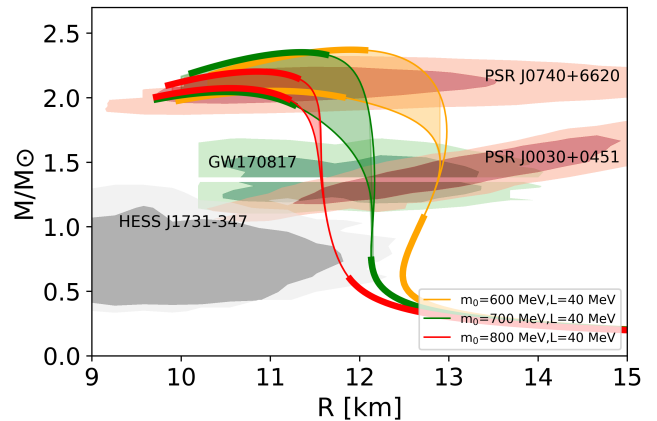


FIG. 7: Mass-Radius relations for $m_0 = 600, 700, 800$ MeV with $L = 40$ MeV. Orange curves are for $(H, g_V)/G = (1.55, 1.3)$ and $(1.45, 0.8)$; green curves for $(H, g_V)/G = (1.6, 1.3)$ and $(1.5, 0.8)$; red curves for $(H, g_V)/G = (1.55, 1)$, $(1.5, 0.8)$.

ACKNOWLEDGEMENT

The work of B.G., and M.H. are supported in part by JSPS KAKENHI Grant Nos. 20K03927, 23H05439 and 24K07045. B.G. is also supported by JST SPRING, Grant No. JPMJSP2125. B.G. would like to take this opportunity to thank the ‘‘Interdisciplinary Frontier Next-Generation Researcher Program of the Tokai Higher Education and Research System.’’

[1] B. P. Abbott (LIGO Scientific Collaboration and Virgo Collaboration), Gw170817: Observation of gravitational

waves from a binary neutron star inspiral, Phys. Rev. Lett. **119**, 161101 (2017).

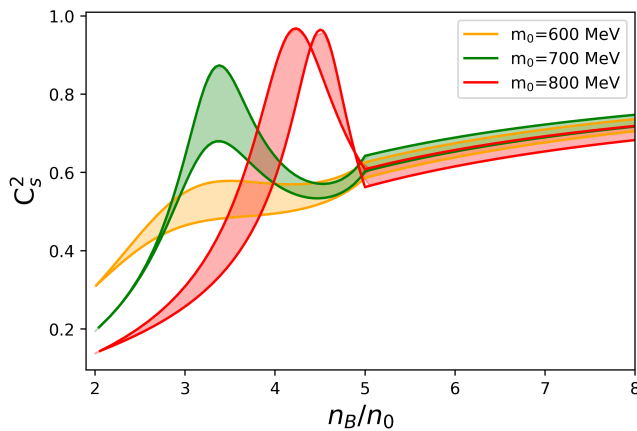


FIG. 8: Sound velocity for $m_0 = 600, 700$ and 800 MeV. The NJL parameters are the same as Fig. 7.

- [2] B. P. Abbott et al. (LIGO Scientific, Virgo, Fermi GBM, INTEGRAL, IceCube, AstroSat Cadmium Zinc Telluride Imager Team, IPN, Insight-Hxmt, ANTARES, Swift, AGILE Team, 1M2H Team, Dark Energy Camera GW-EM, DES, DLT40, GRAWITA, Fermi-LAT, ATCA, ASKAP, Las Cumbres Observatory Group, OzGrav, DWF (Deeper Wider Faster Program), AST3, CAAS-TRO, VINROUGE, MASTER, J-GEM, GROWTH, JAGWAR, CaltechNRAO, TTU-NRAO, NuSTAR, Pan-STARRS, MAXI Team, TZAC Consortium, KU, Nordic Optical Telescope, ePESSTO, GROND, Texas Tech University, SALT Group, TOROS, BOOTES, MWA, CALET, IKI-GW Follow-up, H.E.S.S., LOFAR, LWA, HAWC, Pierre Auger, ALMA, Euro VLBI Team, Pi of Sky, Chandra Team at McGill University, DFN, ATLAS Telescopes, High Time Resolution Universe Survey, RIMAS, RATIR, SKA South Africa/MeerKAT), Multi-messenger Observations of a Binary Neutron Star Merger, *Astrophys. J. Lett.* **848**, L12 (2017), arXiv:1710.05833 [astro-ph.HE].
- [3] B. P. Abbott et al. (LIGO Scientific, Virgo), GW170817: Measurements of neutron star radii and equation of state, *Phys. Rev. Lett.* **121**, 161101 (2018), arXiv:1805.11581 [gr-qc].
- [4] M. C. Miller et al., The Radius of PSR J0740+6620 from NICER and XMM-Newton Data, *Astrophys. J. Lett.* **918**, L28 (2021), arXiv:2105.06979 [astro-ph.HE].
- [5] T. E. Riley et al., A NICER View of the Massive Pulsar PSR J0740+6620 Informed by Radio Timing and XMM-Newton Spectroscopy, *Astrophys. J. Lett.* **918**, L27 (2021), arXiv:2105.06980 [astro-ph.HE].
- [6] V. Doroshenko, V. Suleimanov, G. Pühlhofer, and A. Santangelo, A strangely light neutron star within a supernova remnant, *Nature Astronomy* **6** (2022).
- [7] P.-C. Chu, X.-H. Li, H. Liu, M. Ju, and Y. Zhou, Properties of isospin asymmetric quark matter in quark stars, *Phys. Rev. C* **108**, 025808 (2023).
- [8] P. T. Oikonomou and C. C. Moustakidis, Color-flavor locked quark stars in light of the compact object in the HESS J1731-347 and the GW190814 event, *Phys. Rev. D* **108**, 063010 (2023), arXiv:2304.12209 [astro-ph.HE].
- [9] T. E. Restrepo, C. Providência, and M. B. Pinto, Non-strange quark stars within resummed QCD, *Phys. Rev. D* **107**, 114015 (2023), arXiv:2212.11184 [hep-ph].
- [10] S.-H. Yang, C.-M. Pi, X.-P. Zheng, and F. Weber, Confronting Strange Stars with Compact-Star Observations and New Physics, *Universe* **9**, 202 (2023), arXiv:2304.09614 [astro-ph.HE].
- [11] G. Baym, T. Hatsuda, T. Kojo, P. D. Powell, Y. Song, and T. Takatsuka, From hadrons to quarks in neutron stars: a review, *Rept. Prog. Phys.* **81**, 056902 (2018), arXiv:1707.04966 [astro-ph.HE].
- [12] T. Minamikawa, T. Kojo, and M. Harada, Quark-hadron crossover equations of state for neutron stars: constraining the chiral invariant mass in a parity doublet model, *Phys. Rev. C* **103**, 045205 (2021), arXiv:2011.13684 [nucl-th].
- [13] T. Minamikawa, T. Kojo, and M. Harada, Chiral condensates for neutron stars in hadron-quark crossover: From a parity doublet nucleon model to a Nambu–Jona-Lasinio quark model, *Phys. Rev. C* **104**, 065201 (2021), arXiv:2107.14545 [nucl-th].
- [14] B. Gao, T. Minamikawa, T. Kojo, and M. Harada, Impacts of the U(1)_A anomaly on nuclear and neutron star equation of state based on a parity doublet model, *Phys. Rev. C* **106**, 065205 (2022), arXiv:2207.05970 [nucl-th].
- [15] C. DeTar and T. Kunihiro, Linear sigma model with parity doubling, *Phys. Rev. D* **39**, 2805 (1989).
- [16] D. Jido, M. Oka, and A. Hosaka, Chiral Symmetry of Baryons, *Progress of Theoretical Physics* **106**, 873 (2001), <https://academic.oup.com/ptp/article-pdf/106/5/873/5373808/106-5-873.pdf>.
- [17] G. Aarts, C. Allton, S. Hands, B. Jäger, C. Praki, and J.-I. Skullerud, Nucleons and parity doubling across the deconfinement transition, *Phys. Rev. D* **92**, 014503 (2015), arXiv:1502.03603 [hep-lat].
- [18] H. Nishihara and M. Harada, Extended Goldberger-Treiman relation in a three-flavor parity doublet model, *Phys. Rev. D* **92**, 054022 (2015), arXiv:1506.07956 [hep-ph].
- [19] H.-X. Chen, V. Dmitrasinovic, and A. Hosaka, Baryon fields with U(L)(3) X U(R)(3) chiral symmetry II: Axial currents of nucleons and hyperons, *Phys. Rev. D* **81**, 054002 (2010), arXiv:0912.4338 [hep-ph].
- [20] H.-X. Chen, V. Dmitrasinovic, and A. Hosaka, Baryon Fields with $U_L(3) \times U_R(3)$ Chiral Symmetry III: Interactions with Chiral $(3, \bar{3}) + (\bar{3}, 3)$ Spinless Mesons, *Phys. Rev. D* **83**, 014015 (2011), arXiv:1009.2422 [hep-ph].
- [21] H.-X. Chen, V. Dmitrasinovic, and A. Hosaka, *mathrmBaryonswith* $U_L(3) \times U_R(3)$ Chiral Symmetry IV: Interactions with Chiral $(8, 1) \oplus (1, 8)$ Vector and Axial-vector Mesons and Anomalous Magnetic Moments, *Phys. Rev. C* **85**, 055205 (2012), arXiv:1109.3130 [hep-ph].
- [22] T. Minamikawa, B. Gao, T. Kojo, and M. Harada, Parity doublet model for baryon octets: diquark classifications and mass hierarchy based on the quark-line diagram, (2023), arXiv:2306.15564 [hep-ph].
- [23] T. Hatsuda and M. Prakash, Parity doubling of the nucleon and first-order chiral transition in dense matter, *Physics Letters B* **224**, 11 (1989).
- [24] D. Zschesche, L. Tolos, J. Schaffner-Bielich, and R. D. Pisarski, Cold, dense nuclear matter in a su(2) parity doublet model, *Phys. Rev. C* **75**, 055202 (2007).

- [25] V. Dexheimer, S. Schramm, and D. Zschesche, Nuclear matter and neutron stars in a parity doublet model, *Phys. Rev. C* **77**, 025803 (2008).
- [26] C. Sasaki and I. Mishustin, Thermodynamics of dense hadronic matter in a parity doublet model, *Phys. Rev. C* **82**, 035204 (2010).
- [27] C. Sasaki, H. K. Lee, W.-G. Paeng, and M. Rho, Conformal anomaly and the vector coupling in dense matter, *Phys. Rev. D* **84**, 034011 (2011).
- [28] S. Gallas, F. Giacosa, and G. Pagliara, Nuclear matter within a dilatation-invariant parity doublet model: The role of the tetraquark at nonzero density, *Nuclear Physics A* **872**, 13 (2011).
- [29] J. Steinheimer, S. Schramm, and H. Stöcker, Hadronic $su(3)$ parity doublet model for dense matter and its extension to quarks and the strange equation of state, *Phys. Rev. C* **84**, 045208 (2011).
- [30] W.-G. Paeng, H. K. Lee, M. Rho, and C. Sasaki, Dilaton-limit fixed point in hidden local symmetric parity doublet model, *Phys. Rev. D* **85**, 054022 (2012).
- [31] V. Dexheimer, J. Steinheimer, R. Negreiros, and S. Schramm, Hybrid stars in an $su(3)$ parity doublet model, *Phys. Rev. C* **87**, 015804 (2013).
- [32] W.-G. Paeng, H. K. Lee, M. Rho, and C. Sasaki, Interplay between ω -nucleon interaction and nucleon mass in dense baryonic matter, *Phys. Rev. D* **88**, 105019 (2013).
- [33] A. Mukherjee, J. Steinheimer, and S. Schramm, Higher-order baryon number susceptibilities: Interplay between the chiral and the nuclear liquid-gas transitions, *Phys. Rev. C* **96**, 025205 (2017).
- [34] D. Suenaga, Examination of $N^*(1535)$ as a probe to observe the partial restoration of chiral symmetry in nuclear matter, *Phys. Rev. C* **97**, 045203 (2018).
- [35] Y. Takeda, Y. Kim, and M. Harada, Catalysis of partial chiral symmetry restoration by Δ matter, *Phys. Rev. C* **97**, 065202 (2018).
- [36] H. Abuki, Y. Takeda, and M. Harada, Dual chiral density waves in nuclear matter, *EPJ Web Conf.* **192**, 00020 (2018).
- [37] M. Marczenko, D. Blaschke, K. Redlich, and C. Sasaki, Parity doubling and the dense-matter phase diagram under constraints from multi-messenger astronomy, *Universe* **5**, 10.3390/universe5080180 (2019).
- [38] Y. Motohiro, Y. Kim, and M. Harada, Asymmetric nuclear matter in a parity doublet model with hidden local symmetry, *Phys. Rev. C* **92**, 025201 (2015).
- [39] T. Yamazaki and M. Harada, Constraint to chiral invariant masses of nucleons from gw170817 in an extended parity doublet model, *Phys. Rev. C* **100**, 025205 (2019).
- [40] T. Minamikawa, T. Kojo, and M. Harada, Quark-hadron crossover equations of state for neutron stars: Constraining the chiral invariant mass in a parity doublet model, *Phys. Rev. C* **103**, 045205 (2021).
- [41] A. Mukherjee, S. Schramm, J. Steinheimer, and V. Dexheimer, The application of the Quark-Hadron Chiral Parity-Doublet Model to neutron star matter, *Astrophys. J.* **608**, A110 (2017), arXiv:1706.09191 [nucl-th].
- [42] M. Harada and T. Yamazaki, Charmed mesons in nuclear matter based on chiral effective models, proceedings of the 8th international conference on quarks and nuclear physics (qnp2018).
- [43] M. Marczenko, K. Redlich, and C. Sasaki, Chiral symmetry restoration and Δ matter formation in neutron stars, *Phys. Rev. D* **105**, 103009 (2022), arXiv:2203.00269 [nucl-th].
- [44] T. Minamikawa, B. Gao, T. Kojo, and M. Harada, Chiral Restoration of Nucleons in Neutron Star Matter: Studies Based on a Parity Doublet Model, *Symmetry* **15**, 745 (2023), arXiv:2302.00825 [nucl-th].
- [45] M. Marczenko, D. Blaschke, K. Redlich, and C. Sasaki, Parity Doubling and the Dense Matter Phase Diagram under Constraints from Multi-Messenger Astronomy, *Universe* **5**, 180 (2019), arXiv:1905.04974 [nucl-th].
- [46] Y. K. Kong, T. Minamikawa, and M. Harada, Neutron star matter based on a parity doublet model including the $a_0(980)$ meson, *Phys. Rev. C* **108**, 055206 (2023), arXiv:2306.08140 [nucl-th].
- [47] B.-A. Li, B.-J. Cai, W.-J. Xie, and N.-B. Zhang, Progress in constraining nuclear symmetry energy using neutron star observables since gw170817, *Universe* **7**, 10.3390/universe7060182 (2021).
- [48] G. Baym, S. Furusawa, T. Hatsuda, T. Kojo, and H. Togashi, New Neutron Star Equation of State with Quark-Hadron Crossover, *Astrophys. J.* **885**, 42 (2019), arXiv:1903.08963 [astro-ph.HE].
- [49] T. Hatsuda and T. Kunihiro, QCD phenomenology based on a chiral effective Lagrangian, *Phys. Rept.* **247**, 221 (1994), arXiv:hep-ph/9401310.
- [50] R. C. Tolman, Static solutions of Einstein's field equations for spheres of fluid, *Phys. Rev.* **55**, 364 (1939).
- [51] J. R. Oppenheimer and G. M. Volkoff, On massive neutron cores, *Phys. Rev.* **55**, 374 (1939).
- [52] T. Kojo, QCD equations of state and speed of sound in neutron stars, *AAPPS Bull.* **31**, 11 (2021), arXiv:2011.10940 [nucl-th].
- [53] G. Baym, C. Pethick, and P. Sutherland, The Ground state of matter at high densities: Equation of state and stellar models, *Astrophys. J.* **170**, 299 (1971).
- [54] C. Drischler, R. J. Furnstahl, J. A. Melendez, and D. R. Phillips, How Well Do We Know the Neutron-Matter Equation of State at the Densities Inside Neutron Stars? A Bayesian Approach with Correlated Uncertainties, *Phys. Rev. Lett.* **125**, 202702 (2020), arXiv:2004.07232 [nucl-th].
- [55] I. Tews, J. M. Lattimer, A. Ohnishi, and E. E. Kolomeitsev, Symmetry Parameter Constraints from a Lower Bound on Neutron-matter Energy, *Astrophys. J.* **848**, 105 (2017), arXiv:1611.07133 [nucl-th].
- [56] K. Masuda, T. Hatsuda, and T. Takatsuka, Hadron-Quark Crossover and Massive Hybrid Stars with Strangeness, *Astrophys. J.* **764**, 12 (2013), arXiv:1205.3621 [nucl-th].
- [57] K. Masuda, T. Hatsuda, and T. Takatsuka, Hadron-quark crossover and massive hybrid stars, *PTEP* **2013**, 073D01 (2013), arXiv:1212.6803 [nucl-th].
- [58] G. Baym, T. Hatsuda, T. Kojo, P. D. Powell, Y. Song, and T. Takatsuka, From hadrons to quarks in neutron stars: a review, *Reports on Progress in Physics* **81**, 056902 (2018).
- [59] M. Marczenko, L. McLerran, K. Redlich, and C. Sasaki, Reaching percolation and conformal limits in neutron stars, *Phys. Rev. C* **107**, 025802 (2023), arXiv:2207.13059 [nucl-th].
- [60] P. Braun-Munzinger, A. Kalweit, K. Redlich, and J. Stachel, Confronting fluctuations of conserved charges in central nuclear collisions at the LHC with predictions from Lattice QCD, *Phys. Lett. B* **747**, 292 (2015), arXiv:1412.8614 [hep-ph].

- [61] B. Dey, C. A. Meyer, M. Bellis, and M. Williams (CLAS), Data analysis techniques, differential cross sections, and spin density matrix elements for the reaction $\gamma p \rightarrow \phi p$, Phys. Rev. C **89**, 055208 (2014), [Addendum: Phys.Rev.C 90, 019901 (2014)], arXiv:1403.2110 [nucl-ex].
- [62] T. Mibe, W. C. Chang, T. Nakano, D. S. Ahn, J. K. Ahn, H. Akimune, Y. Asano, S. Daté, H. Ejiri, H. Fujimura, M. Fujiwara, K. Hicks, T. Hotta, K. Imai, T. Ishikawa, T. Iwata, H. Kawai, Z. Y. Kim, K. Kino, H. Kohri, N. Kumagai, S. Makino, T. Matsuda, T. Matsumura, N. Matsuoka, K. Miwa, M. Miyabe, Y. Miyachi, M. Morita, N. Muramatsu, M. Niiyama, M. Nomachi, Y. Ohashi, T. Ooba, H. Ohkuma, D. S. Oshuev, C. Rangacharyulu, A. Sakaguchi, T. Sasaki, P. M. Shagin, Y. Shiino, H. Shimizu, Y. Sugaya, M. Sumihama, A. I. Titov, Y. Toi, H. Toyokawa, A. Wakai, C. W. Wang, S. C. Wang, K. Yonehara, T. Yorita, M. Yoshimura, M. Yosoi, and R. G. T. Zegers (LEPS Collaboration), Near-threshold diffractive ϕ -meson photo-production from the proton, Phys. Rev. Lett. **95**, 182001 (2005).